

# 旁路耦合微束等离子弧热特性及焊缝成形特点

李挺<sup>1</sup>, 黄健康<sup>1</sup>, 陈秀娟<sup>2</sup>, 余淑荣<sup>2</sup>, 樊丁<sup>1</sup>

(1. 兰州理工大学 有色金属先进加工与再利用省部共建国家重点实验室, 兰州 730050;  
2. 兰州理工大学 机电工程学院, 兰州 730050)

**摘要:** 针对传统微束等离子弧焊中焊丝熔敷率与焊接电流不能解耦的局限, 提出旁路耦合微束等离子弧焊方法。通过给外填焊丝添加一电流, 使焊丝与焊枪钨极间产生一个旁路电弧, 实现熔化母材热量与熔化焊丝热量的解耦, 确保熔化母材电流稳定的同时提高填充焊丝的熔化速度。对旁路耦合微束等离子弧焊的熔敷率、母材热输入及焊缝成形质量进行试验研究。结果表明, 该方法既保持了传统微束等离子弧焊的优点, 又在提高焊丝熔敷率的同时降低母材的热输入; 并在其它焊接参数保持不变时, 随旁路电流的增加, 焊缝的熔宽、熔深和稀释率减小, 余高和成形系数增大。

**关键词:** 旁路耦合微束等离子弧焊; 旁路电流; 热输入

中图分类号: TG 409

文献标识码: A

doi: 10.12073/j.hjxb.2018390224

## 0 序 言

微束等离子弧焊是一种小电流的焊接方法, 它是在等离子弧焊的基础上, 采用小孔径喷嘴进一步加强对电弧的压缩, 并利用联合型电弧及等离子弧温度高的特点, 使微束等离子弧能够稳定存在。与钨极氩弧焊相比, 微束等离子弧焊可焊接更薄的金属, 最小可焊接厚度为 0.01 mm; 电弧挺度和稳定性更好, 对弧长的变化不敏感, 弧长可以在很大范围内变化而不会断弧; 并且焊缝窄、热影响区小、焊缝变形小<sup>[1]</sup>。微束等离子弧焊的应用范围非常广泛, 已经成功应用于航空、航天、造船、医学等许多领域<sup>[2]</sup>, 特别适合于金属薄壁件<sup>[3-5]</sup>、金属细丝筛网<sup>[6]</sup>及高温合金<sup>[7]</sup>的焊接。陈焕明等人<sup>[8]</sup>研制的变极性微束等离子弧焊电源能够有效减少钨极烧损, 控制阴极清理作用, 适合于铝合金的焊接, 并且一些学者在变极性等离子弧焊焊接铝合金方面做了深入的研究<sup>[9-12]</sup>。柴国明等人<sup>[13]</sup>对添加活性剂后的等离子电弧特性和电弧力进行了研究, 发现电弧温度分布更加紧凑, 电弧力分布半径减小, 压力峰值增大。武传松等人<sup>[14]</sup>通过数值模拟研究了等离子弧焊穿孔过程中熔池流动和传热过程, 展示了小孔形成前后流场和

温度场的演变规律。但是在实际焊接中当工件对接间隙稍大时, 微束等离子弧焊常出现焊缝余高不够或下陷, 也容易出现咬边的缺陷, 这就说明焊缝填充金属不足, 需要填充焊丝, 而微束等离子弧焊电流很小, 形成的熔池也很小, 焊丝熔化速度不高, 影响生产效率。

为了提高微束等离子弧焊生产效率及实现熔化母材热量与熔化焊丝热量的解耦控制, 提出旁路耦合微束等离子弧焊 (double-electrode micro-plasma arc welding, DE-MPAW)。通过理论分析及所做的相关试验表明所提出的方法的可行性和有效性。

## 1 DE-MPAW 原理

旁路耦合微束等离子弧焊主要由主路等离子焊枪和旁路熔化极焊枪组成, 其基本原理如图 1 所示。该方法采用一台陡降特性微束等离子焊机, 焊机的负极与微束等离子焊枪连接, 焊机的工件正极同时与工件和旁路熔化极焊枪连接。焊接时微束等离子焊机在微束等离子焊枪与工件之间提供一定的电压、电流, 使气体电离产生主弧, 同时当旁路焊丝送进接触到主路电弧时, 由于主路等离子电弧温度很高, 伸长的焊丝迅速熔化蒸发产生金属蒸气, 又由于微束等离子焊机在等离子焊枪与焊丝间也提供了一定的电压与电流, 因此在焊枪与焊丝之间

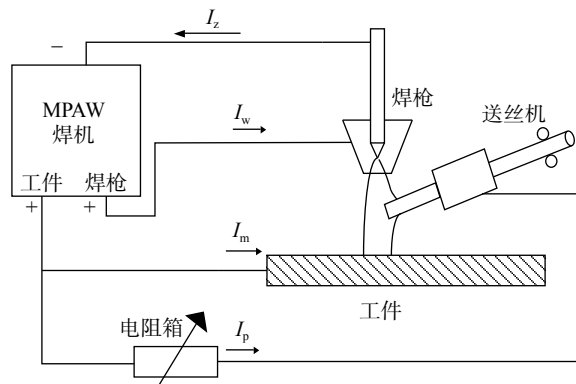


图 1 DE-MPAW 原理示意图

Fig. 1 Schematic diagram of DE-MPAW principle

又产生了旁路电弧, 等离子主弧与旁路电弧形成一个耦合电弧。这样在焊接过程中电流从焊机工件正极流出后分为两个部分, 一部分流入母材, 一部分流经电阻器后通过焊丝进行分流。因此流入母材的电流并不等于流过焊枪的电流, 而是等于流经焊枪钨极的电流减去旁路焊丝分流的电流及维弧电流, 旁路耦合微束等离子弧焊焊接过程中的电流关系如式(1)所示, 即

$$I_z = I_m + I_p + I_w \quad (1)$$

式中:  $I_m$  为流入母材的电流;  $I_z$  为流过焊枪钨极的电流;  $I_p$  为流过焊丝的旁路电流;  $I_w$  为维弧电流。

对于主路电弧, 由于工件接微束等离子焊机的工件正极, 微束等离子焊枪的钨极接焊机的负极, 焊枪钨极与工件产生的主路电弧为微束等离子弧, 保留了微束等离子弧的特点; 对于旁路电弧, 旁路焊丝接微束等离子焊机的正极, 产生主路电弧后主路等离子弧的正离子就成为了旁路电弧的正极, 旁路焊丝与工件的距离远小于旁路焊丝与焊枪钨极

的距离, 根据电压最小原理, 旁路电弧为了保持最小的能量消耗, 只会在旁路焊丝与主路微束等离子弧柱区之间最短的距离内燃烧, 并且旁路耦合微束等离子弧焊是在微束等离子弧焊的基础上采用单个微束等离子弧焊机改进而来的, 而微束等离子弧焊机是下降特性的电源, 因此旁路电弧的自调节作用较弱, 不能仅依靠电弧的自调节作用保持旁路焊丝送进与熔化的平衡并保持旁路电弧的稳定燃烧, 此时需要依靠弧压反馈进行旁路焊丝送丝速度的控制, 从而保证旁路电弧的稳定燃烧。所以该焊接方法既有微束等离子弧焊的特性, 又有旁路耦合电弧焊热输入可调控的特性。

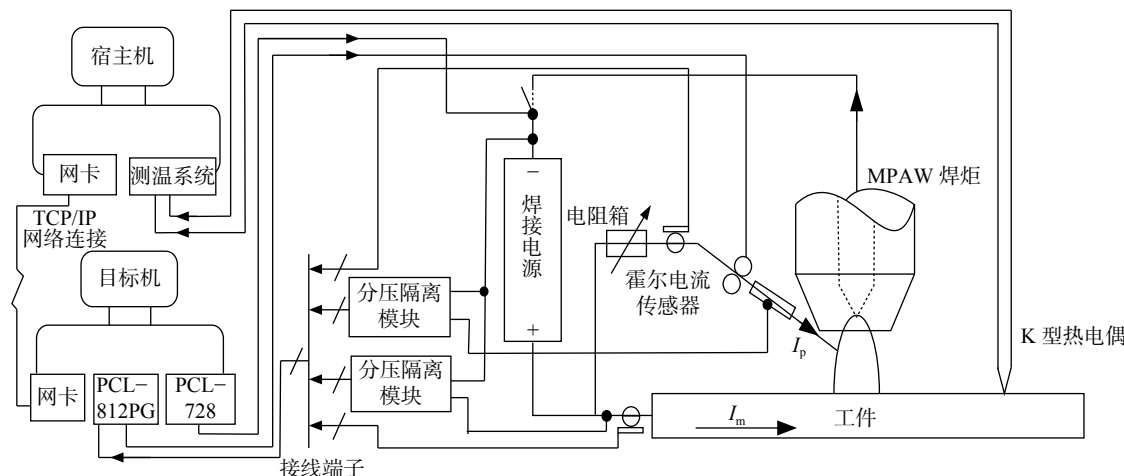
## 2 试验系统与方法

### 2.1 试验系统组成

旁路耦合微束等离子弧焊试验系统如图 2 所示, 主要包括焊接系统、焊接辅助系统和信号采集与传感系统。其中, 焊接系统由 LHM-50 精密微束等离子弧焊机和 WF-007A 多功能自动氩弧填丝机组成; 焊接辅助系统包括三轴数控工作平台、步进电动机和驱动器、PCLD-885 固态继电器卡等; 信号采集与传感系统由工控机、PCL-812PG 数据采集卡、PCL-728 模拟量输出卡、霍尔电流传感器、电压隔离模块、K型热电偶、ADAM-4018 温度采集模块及配套的温度采集软件等组成。

### 2.2 试验方法

试验母材采用厚度为 3 mm 的 304 不锈钢板, 焊丝采用直径为 0.8 mm 的 ER304L 不锈钢焊丝。焊前用砂纸打磨并用丙酮清洗不锈钢板, 以除去表



(C)1994-2020 China Academic Journal Electronic Publishing House. All rights reserved. <http://www.cnki.net>  
Fig. 2 Experiment system of DE-MPAW

面污渍。

试验采用旁路耦合微束等离子弧焊在平板上堆焊的方式进行,如图3所示,焊接过程中,两把焊枪固定在一起相对于试验平台静止,工件运动。沿焊接方向上,GMAW焊枪在前,MPAW焊枪在后。其中,焊接总电流为50 A、保护气体流量为10 L/min、离子气体流量0.6 L/min、送丝速度280 cm/min、等离子弧长10 mm,在整个试验过程中保持不变。

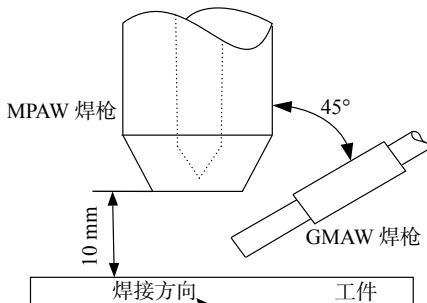


图3 DE-MPAW 焊枪组合  
Fig. 3 Torch-set of DE-MPAW

### 3 试验结果与分析

#### 3.1 DE-MPAW 熔敷率分析

在其它参数不变的前提下,分别在旁路电流为0 A和旁路电流为14 A时逐渐增大焊接速度进行焊接试验,得到如图4和图5所示的焊缝形貌。

由图4可知,在旁路电流为0 A、焊接速度为190 mm/min时焊缝成形良好,而当焊接速度达到210 mm/min时出现明显的驼峰焊道;由图5可知,旁路电流为14 A、焊接速度为250 mm/min时焊缝成形依然良好,而当焊接速度达到270 mm/min时出现连续的驼峰焊道。这是因为在高速焊接过程中,焊接电流过大产生过高的电弧压力是产生驼峰焊道的主要原因,但是如果能够保证单位长度焊缝上熔敷的填充金属量恒定,并实现母材与焊丝热输



(a) 焊接速度 190 mm/min



(b) 焊接速度 210 mm/min

(C)1994-2020 China Academic Electronic Publishing House. All rights reserved. <http://www.cnki.net>  
Fig. 4 Weld formation under bypass current 0 A



(a) 焊接速度 250 mm/min



(b) 焊接速度 270 mm/min

图5 旁路电流 14 A 的焊缝成形  
Fig. 5 Weld formation under bypass current 14 A

入的合理分配,即保证焊丝熔敷率的同时保持母材熔深不变,就能有效控制驼峰焊道等缺陷的产生。而旁路耦合微束等离子弧焊中电流较小又经旁路焊丝的分流,从而在保证焊丝高熔敷率的同时进一步降低了熔化母材的电流,所以不易出现驼峰焊道,直到焊接速度过快,熔化的焊丝不能填满熔池,才导致驼峰焊道的产生。

在焊丝熔敷率方面,常规微束等离子弧焊中熔化焊丝的热量主要来源于熔池的热传递,焊丝熔敷效率受到限制;热丝MPAW中增加了一个电源利用焊丝电阻热 $P_w$ 对焊丝进行预热,提高了焊丝熔敷率。如式(2),即

$$P_w = I_w^2 R_w = I_w U_w \quad (2)$$

式中: $P_w$ 为电阻热功率; $I_w$ 为通过焊丝的电流; $R_w$ 为焊丝伸出长度的电阻; $U_w$ 焊丝上的电压。而在旁路耦合微束等离子弧焊中,焊丝电阻热仍然存在,但是又增加了由于阳极压降引起的热 $I_w U_a$ , $U_a$ 为阳极压降,因此旁路耦合微束等离子弧焊焊丝的熔敷率就是热丝MPAW的 $k$ 倍。如式(3),即

$$k = \frac{I_w U_w + I_w U_a}{I_w U_w} = 1 + \frac{U_a}{U_w} \quad (3)$$

焊丝伸出长度的电阻 $R_w$ 非常小,因此在小电流焊接时焊丝伸出长度上分担的电压 $U_w = I_w R_w$ 远远小于阳极压降 $U_a$ 。

#### 3.2 DE-MPAW 热输入分析

采用如表1所示的焊接参数,进行DE-MPAW热循环曲线测试试验,如图6所示,测试时将3个K型热电偶利用焊偶仪焊接在母材正面的3个点上,各点距离焊缝中心线的距离分别为10, 20, 30 mm。

测试得到的热循环曲线如图7所示,各参数的热循环曲线测试结果统计如表2所示。在四组试验得到的热循环曲线上,旁路电流为0 A时的距离焊缝中心线最近的A点峰值温度最高,达到538.5 °C,

表1 热循环曲线测试焊接参数

Table 1 Welding parameters of thermal cycling curve

编号	母材电压 $U_m/V$	母材电流 $I_m/A$	旁路电压 $U_p/V$	旁路电流 $I_p/A$	焊接速度 $v/(mm \cdot min^{-1})$
1	26.96	50	0	0	90
2	26.86	40	22.52	10	90
3	25.96	38	23.21	12	90
4	25.72	36	24.38	14	90

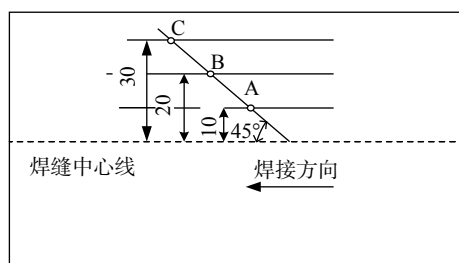


图6 热电偶测量点的分布图 (mm)

Fig. 6 Distribution of thermocouple measurement points

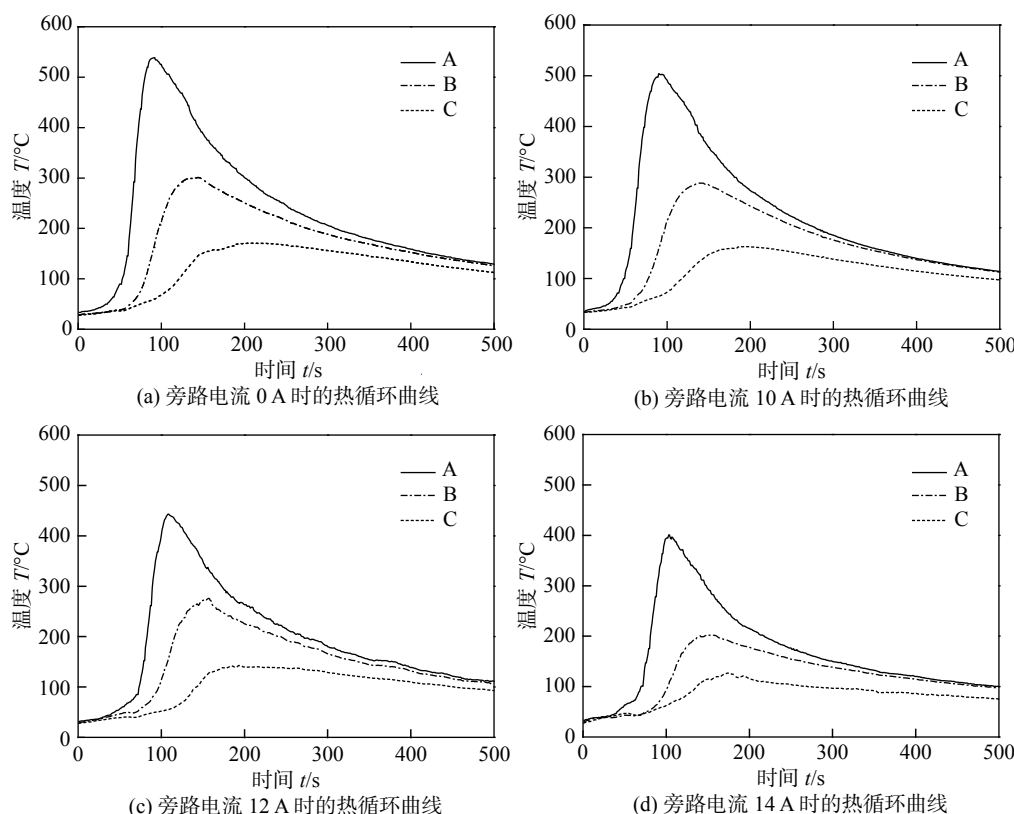


图7 不同旁路电流下的热循环曲线

Fig. 7 Thermal cycling curves under different bypass currents

入的程度,所以DE-MPAW具有较低的母材热输入.

### 3.3 DE-MPAW 焊缝成形分析

对测量热循环曲线后的四条焊缝进行切割、腐蚀处理,得到如图8所示的焊缝截面形貌,并对每条焊缝的熔宽、熔深和余高分别进行了测量统计,

随着旁路电流从10 A增加到12, 14 A, A点的温度峰值依次减小为504, 442.9, 401.1 °C, 而B点和C点的峰值温度也符合这一变化趋势. 由图7和表2可以看出, 随着旁路电流的增大, 母材的热输入是逐渐降低的. 这是因为在焊接过程中母材的热输入主要有三种形式: 焊接电弧面热源直接加热母材、熔滴体热源将热量带入熔池、流过母材的电流产生电阻热. 对于DE-MPAW, 熔化母材的电流 $I_m$ 和焊接总电流 $I_z$ 遵循(1)式的关系,  $I_m$ 明显要小于 $I_z$ , 因此主路等离子弧和旁路电弧耦合形成的耦合电弧对母材的热输入比常规的MPAW要低很多; 引入旁路电弧后, 旁路焊丝上产生熔滴, 进而将热量带入母材, 这样母材的热输入比只依靠等离子弧和熔池熔化焊丝的常规MPAW的高; 但是由于旁路电弧的分流作用, 使流经母材电流显著减小, 母材上产生的电阻热也显著减小, 耦合电弧和母材电阻热对母材热输入减小的程度要大于熔滴增加母材热输

如图9所示. 根据测量的焊缝几何参数进一步又计算了各焊缝的成形系数和稀释率, 如图10所示.

由图9可以看出, 随着旁路电流的增加, 焊缝熔宽、熔深逐渐减小, 余高逐渐增大. 由图10可知, 随旁路电流的增大, 成形系数增大, 稀释率减小. 这

表2 不同旁路电流下各测试点峰值温度

Table 2 Peak temperature of each test point under different bypass currents

旁路电流 $I_p/A$	A点峰值温度 $T_{fa}/^{\circ}\text{C}$	B点峰值温度 $T_{fb}/^{\circ}\text{C}$	C点峰值温度 $T_{fc}/^{\circ}\text{C}$
0	538.5	300.9	170.8
10	504.0	288.2	162.8
12	442.9	276.2	140.0
14	401.1	202.8	121.7

是由于焊缝的熔宽与主弧电压相关,主弧电压随旁路电流的增大而缓慢降低,因此熔宽也缓慢减小。



(a) 旁路电流 0 A 时的焊缝截面形貌



(b) 旁路电流 10 A 时的焊缝截面形貌



(c) 旁路电流 12 A 时的焊缝截面形貌



(d) 旁路电流 14 A 时的焊缝截面形貌

图8 不同旁路电流下的焊缝截面形貌

Fig. 8 Weld cross-section under different bypass currents

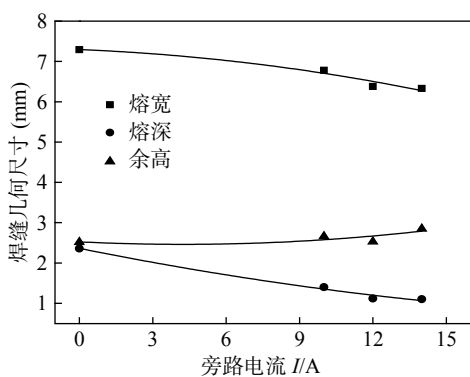


图9 焊缝几何参数随旁路电流的变化情况

Fig. 9 Variation of weld geometry parameters with bypass current

#### 4 结论

(C)1994-2020 China Academic Journal Electronic Publishing House. All rights reserved. <http://www.cnki.net>  
(1)DE-MPAW 相对于传统及热丝 MPAW 具有

由于旁路电弧分走了一部分熔化母材的电流,使得作用在熔池表面的电弧压力减小,并且引入旁路电弧后,焊丝在未插入到等离子弧中心时就已经熔化形成熔滴,熔滴过渡的路径偏离等离子弧中心而偏向旁路一侧,熔滴落在熔池稍靠前的位置,熔滴对熔池的冲击力作用点与电弧压力的作用点发生偏离,且熔池前端液态金属层较厚,对熔滴冲击力的缓冲作用较大,因此随着旁路电流的增大,熔深减小,稀释率降低。熔宽减小的速率小于熔深减小的速率,所以焊缝成形系数随旁路电流的增大略有增加,这有利于增强抗热裂纹性能,利于薄板高速焊及异种金属的焊接。



(a) 旁路电流 0 A 时的焊缝截面形貌



(b) 旁路电流 10 A 时的焊缝截面形貌



(c) 旁路电流 12 A 时的焊缝截面形貌

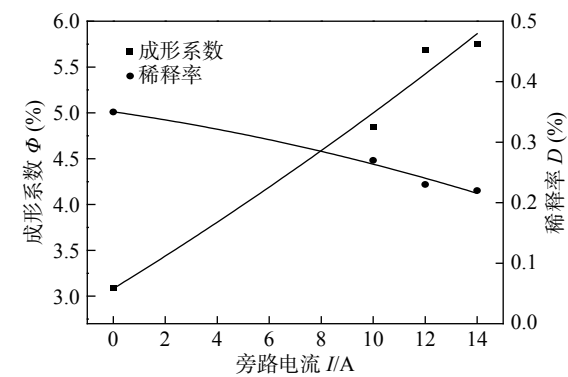


图10 成形系数和稀释率随旁路电流的变化情况

Fig. 10 Variation of forming coefficient and dilution rate with bypass current

较高的焊丝熔敷率和焊接速度,较低的母材热输入,可以实现熔化母材的热量与熔化焊丝的热量的解耦。

(2) 在其它焊接参数保持不变时, 随旁路电流的增加, 焊缝的熔宽、熔深和稀释率减小, 余高和成形系数增大。

## 参考文献:

- [1] 张应立. 特种焊接技术[M]. 北京: 金盾出版社, 2012.
- [2] 陈克选, 李鹤岐, 李春旭. 变极性等离子弧焊研究进展[J]. 焊接学报, 2004, 25(1): 124–128.  
Chen Kexuan, Li Heqi, Li Chunxu. Progress in variable polarity plasma arc welding[J]. Transactions of the China Welding Institution, 2004, 25(1): 124–128.
- [3] 蒋应田, 李宪臣, 李明利. 不锈钢薄壁管的微束脉冲等离子弧焊接工艺[J]. 焊接, 2006(9): 53–56.  
Jiang Yingtian, Li Xianchen, Li Mingli. Pulse micro-plasma arc welding technology of stainless steel thin-wall pipe[J]. Welding & Joining, 2006(9): 53–56.
- [4] Prasad K S, Rao C S, Rao D N. Prediction of weld pool geometry in pulsed current micro plasma arc welding of SS304L stainless steel sheets[J]. International Transaction Journal of Engineering, Management & Applied Sciences & Technologies, 2011, 2(3): 325–336.
- [5] Urena A, Otero E, Utrilla M V, et al. Weldability of a 2205 duplex stainless steel using plasma arc welding[J]. Journal of Materials Processing Technology, 2007, 182(1): 624–631.
- [6] 闫久春, 王小峰, 吕连山, 等. 飞机发动机滤油网组件的高频脉冲微束等离子弧焊[J]. 焊接, 1997(4): 8–10.  
Yan Jiuchun, Wang Xiaofeng, Lü Lianshan et al. High frequency pulse micro-plasma arc welding for oil filter screen of jet engine[J]. Welding & Joining, 1997(4): 8–10.
- [7] 宋文清, 曲 伸, 石坚鲲, 等. GH738 金属封严圈的微束等离子焊接[J]. 电焊机, 2015, 45(8): 97–101.  
Song Wenqing, Qu Shen, Shi Jiankun, et al. Micro-beam plasma welding of GH738 superalloy for a sealing ring of aero-engine turbine[J]. Electric Welding Machine, 2015, 45(8): 97–101.
- [8] 陈焕明, 熊震宇, 江淑园. 微束等离子弧焊变极性电源[J]. 焊接技术, 2000, 29(1): 29–30.  
Chen Huanming, Xiong Zhenyu, Jiang Shuyuan. A variable polarity power supply of micro-plasma arc welding[J]. Welding Technology, 2000, 29(1): 29–30.
- nology, 2000, 29(1): 29–30.
- [9] 陈树君, 蒋 凡, 张俊林, 等. 铝合金变极性等离子弧穿孔横焊焊缝成形规律分析[J]. 焊接学报, 2013, 34(4): 1–6.  
Chen Shujun, Jiang Fan, Zhang Junlin, et al. Principle of weld formation in variable polarity keyhole plasma arc transverse welding of aluminum alloy[J]. Transactions of the China Welding Institution, 2013, 34(4): 1–6.
- [10] 张勤练, 杨春利, 林三宝, 等. 2A14 铝合金变极性等离子横向焊缝成形特点[J]. 焊接学报, 2013, 34(9): 79–82.  
Zhang Qinlian, Yang Chunli, Lin Sanbao, et al. Characteristics of weld formation in variable polarity plasma arc horizontal welding of 2A14 aluminum alloy[J]. Transactions of the China Welding Institution, 2013, 34(9): 79–82.
- [11] 牟取晗, 韩永全, 赵 鹏, 等. 铝合金变极性等离子弧焊应力场数值分析[J]. 焊接学报, 2015, 36(11): 97–100.  
Mou Quahan, Han Yongquan, Zhao Peng, et al. Numerical simulation of stress field in variable polarity plasma arc welding of aluminum alloys[J]. Transactions of the China Welding Institution, 2015, 36(11): 97–100.
- [12] 李国伟, 陈芙蓉, 韩永全, 等. 高强铝合金脉冲变极性等离子弧焊接头组织与性能[J]. 焊接学报, 2016, 37(11): 27–30.  
Li Guowei, Chen Furong, Han Yongquan, et al. Microstructure and mechanical properties of pulse VPPA welded high-strength aluminum alloy joints[J]. Transactions of the China Welding Institution, 2016, 37(11): 27–30.
- [13] 柴国明, 朱铁峰, 张 慧. 活性剂等离子弧焊焊接电弧的特性[J]. 机械工程学报, 2005, 41(10): 170–173.  
Chai Guoming, Zhu Yifeng, Zhang Hui. Property of the arc in activated flux plasma arc welding[J]. Chinese Journal of Mechanical Engineering, 2005, 41(10): 170–173.
- [14] 张 涛, 武传松, 陈茂爱. 穿孔等离子弧焊焊接熔池流动和传热过程的数值模拟[J]. 金属学报, 2012, 48(9): 1025–1032.  
Zhang Tao, Wu Chuansong, Chen Maoai. Modelling fluid flow and heat transfer phenomena in keyholing stage of plasma arc welding[J]. Acta Metallurgica Sinica, 2012, 48(9): 1025–1032.

**作者简介:**李 挺,男,1990年出生,硕士研究生。主要从事焊接智能传感与控制研究。Email: [liting5936@qq.com](mailto:liting5936@qq.com)

**通讯作者:**黄健康,男,1981年出生,博士,副教授,硕士研究生导师。Email: [sr2810@163.com](mailto:sr2810@163.com)

relative motion; microcosmic evolution

**Investigation of brazing joints of Al<sub>2</sub>O<sub>3</sub> ceramics to Kovar alloys by Ti+Nb/Mo metallization** XIN Chenglai, LI Ning, YAN Jiazen (School of Manufacturing Science and Engineering, Sichuan University, Chengdu 610065, China). pp 45-48

**Abstract:** Ti+Nb/Mo thin films were deposited onto Al<sub>2</sub>O<sub>3</sub> ceramic by magnetron sputtering with a subsequent nickel-plating to ensure the robust brazing of Al<sub>2</sub>O<sub>3</sub> ceramic to Kovar alloy using the filler of AgCu28. Microstructures of the metallization layer and the brazing joints of Al<sub>2</sub>O<sub>3</sub>/Kovar were investigated systematically by scanning electron microscopy (SEM) and energy dispersive X-ray (EDS). The results show that the interfacial reaction layers are created between filler alloys and base materials. Interdiffusion of Ni and Cu at the interface of AgCu/Kovar resulted in the formation of the reaction layer. The metallization layer plays an important role in hindering the formation of intermetallic compounds and relieving residual thermal stress at Al<sub>2</sub>O<sub>3</sub>/AgCu interface. In addition, the presence of eutectic region arising from nickel-plating can improve the thickness of the brazing seam and therefore a good bonding between Al<sub>2</sub>O<sub>3</sub> ceramic and Kovar was achieved.

**Key words:** Al<sub>2</sub>O<sub>3</sub> ceramics; metallization; braze joint; magnetron sputtering

**Microstructural evolution of Cu/Sn/Cu joints and effect of temperature on three-dimensional morphology of IMCs in packaging technology** LIANG Xiaobo, LI Xiaoyan, YAO Peng, LI Yang (College of Materials Science and Engineering, Beijing university of technology, Beijing 100124, China). pp 49-54

**Abstract:** A 4 μm thick Sn film was deposited on the copper substrate by electroplating. Two copper substrates with electroplated Sn were constituted of a Cu/Sn/Cu structure. 240 °C and 1 N were chosen as soldering temperature and pressure to be soldered for different time to investigate the law of microstructural evolution of IMCs. The three-dimensional morphology of Cu<sub>6</sub>Sn<sub>5</sub> and Cu<sub>3</sub>Sn under different soldering temperature(240, 270, 300 °C) were fabricated, Investigate the effect of temperature on three-dimensional morphology. The results show Cu<sub>6</sub>Sn<sub>5</sub> was planar after soldered for 30 min and turned into scallop-like with the increase of soldering time. Cu<sub>3</sub>Sn in the bottom of scallop was thicker than that in bottom of scallop on both sides. Sn was reacted with the increase of soldering time, Cu<sub>6</sub>Sn<sub>5</sub> in the two side merged into a whole gradually. Increase more soldering time, Cu<sub>6</sub>Sn<sub>5</sub> continued to be transformed into Cu<sub>3</sub>Sn. The three-dimensional of Cu<sub>6</sub>Sn<sub>5</sub> transformed from polyhedron shape to procumbent and the size of Cu<sub>3</sub>Sn grains decreased gradually with the increase of soldering temperature.

**Key words:** Cu/Sn/Cu joints; Cu<sub>3</sub>Sn; Cu<sub>6</sub>Sn<sub>5</sub>; microstructural evolution; three-dimensional morphology

**Thermal characteristics and weld formation of double-electrode micro-plasma arc welding** LI Ting<sup>1</sup>, HANG Jiankang<sup>1</sup>, CHEN Xiujuan<sup>2</sup>, YU Shurong<sup>2</sup>, FAN Ding<sup>1</sup> (1.

State Key Laboratory of Advanced Processing and Recycling Publishing Abstract: All rights reserved. <http://www.weld.net>

of Non-ferrous Metals, Lanzhou University of Technology, Lanzhou 730050, China; 2. School of Mechanical and Electronic Engineering, Lanzhou University of Technology, Lanzhou 730050, China). pp 55-60

**Abstract:** To solve the limitation about deposition rate and welding current can not be decoupled of the traditional micro-plasma arc welding, double-electrode micro plasma arc welding is proposed. The article added a bypass current into the filler wire to make a bypass arc is appeared between the wire and the tungsten. Though this method to realize the decoupling of the heat of melting base material and the heat of melting wire. Thus, the melting speed of the filler wire is increased while the current of melting base material keeps stable. The experimental study was carried out on the deposition rate, the heat input of the base metal and the weld formation quality of the double-electrode micro plasma arc welding. The double-electrode micro plasma arc welding not only maintains the advantages of the conventional micro plasma arc welding, but also improves the deposition rate and reduces the heat input of the base metal; When the other welding parameters remain unchanged, , the weld penetration and dilution rate decrease and the forming coefficient increases with the increase of the bypass current.

**Key words:** double-electrode micro plasma arc welding; bypass current; heat input

**Detection of non-groove butt joint feature based on corner principle** WANG Wenchoao, GAO Xiangdong, DING Xiaodong, ZHANG Nanfeng (Guangdong Provincial Welding Engineering Technology Research Center, Guangdong University of Technology, Guangzhou 510006, China). pp 61-64

**Abstract:** A method for detecting and tracking the non-groove butt joint by using the principle of corner detection based on line structured light vision sensing is studied. It is different from the traditional line structured light sensing method to detect the weld position according to the deformation feature. The proposed method applies for the fact that the laser stripe has obvious gray gradient variation in the weld. The morphological image processing method is adopted to extract the feature of weld center. The gray value of each column in the image is calculated, and the region of interest is extracted by the central difference method. According to the principle of the corner detection method, the sub-pixel coordinates of the weld center can be determined accurately. The actual position deviation of the weld is obtained by using a simple and fast system calibration. Experimental results show that the average error can be kept within 0.1 mm by tracking a butt joint whose width is about 0.2 mm, which can meet the requirement of seam tracking precision.

**Key words:** seam tracking; line structured light; butt joint weld; non-groove; corner detection

**Superplastic deformation mechanism of acicular weld microstructure of titanium alloy** JIANG Xunyan, CHENG Donghai, CHEN Yiping, HU Dean (Aviation Manufacturing and Engineering College, Nanchang Hangkong University, Nanchang 330063, China). pp 65-70

Abstract: All rights reserved. <http://www.weld.net>